



CrossMark
 click for updates

Cite this: *RSC Adv.*, 2016, 6, 64003

Highly efficient orange phosphorescent organic light-emitting diodes based on an iridium(III) complex with diethyldithiocarbamate (S^{AS}) as the ancillary ligand[†]

Qunbo Mei,^{*a} Chen Chen,^a Ruqiang Tian,^a Min Yang,^a Bihai Tong,^b Qingfang Hua,^a Yujie Shi,^a Quli Fan^a and Shanghui Ye^{*a}

A novel iridium(III) complex Ir(dpp)₂(dta) (dppH = 4,6-diphenyl pyrimidine; dta = diethyldithiocarbamate) was synthesized and characterized. The complex displayed strong emissions at 575 nm with high photoluminescence quantum yields of 86% in the doped poly(methyl methacrylate) (PMMA) film at 1% doping concentration. The orange-yellow polymer light-emitting devices (PLEDs) based on Ir(dpp)₂(dta) as a triplet emitter with different concentrations (x = 1%, 3%, 5%, 7% and 10%) doped in a polymeric host 70% poly(N-vinylcarbazole) (PVK) + 30% 2,2'-(1,3-phenylene)bis[5-(4-tert-butylphenyl)-1,3,4-oxadiazole] (OXD-7) were fabricated with high luminance and efficiency. The device achieved an ideal turn-on voltage (<4 V) and superior luminance (81 918 cd m⁻²) as well as electroluminescence efficiency (30.12 cd A⁻¹) at 3% doping concentration.

Received 13th May 2016
 Accepted 24th June 2016

DOI: 10.1039/c6ra12529h

www.rsc.org/advances

Introduction

Organic light-emitting diodes (OLEDs) have become a hot research field and have attracted great attention due to their potential applications in organic flat-panel displays since Tang reported efficient electroluminescence by using tris(8-hydroxyquinolino) aluminium (AlQ₃) as an emitter in the first efficient small molecule OLEDs in 1987.¹ The organic electrophosphorescent materials play a critical role because they can fully utilize both singlet and triplet excitons through the strong spin-orbital coupling caused by heavy metal ions in complexes. Theoretically, the internal quantum efficiency of the phosphorescent OLEDs (PhOLEDs) can reach up to 100%.² Among these emitting materials for OLEDs, iridium(III) complexes are the most promising candidates. Iridium(III) complexes are usually constituted by three bidentate ligands, either homoleptic (C^N)₃Ir or heteroleptic (C^N)₂Ir(L^X), where C^N represents a cyclometalating bidentate ligand and L^X

stands for an ancillary bidentate ligand.³ In general, the cyclometalating ligands (C^N) are usually aromatic heterocyclic rings containing C, N, S, O atoms, *etc.*⁴ Aromatic heterocyclic compounds containing N atoms such as pyrimidine derivatives and pyridine derivatives are expected to be electron-deficient units which have been used to construct novel cyclometalated organic ligand and electron-transporting materials.⁵ In 2003, Tsuboyama *et al.* designed and synthesized a series of neutral facial homoleptic cyclometalated iridium(III) complexes based on pyridine derivatives cyclometalating ligands (C^N) for use as red-emissive materials in OLEDs.⁶ Cyclometalated organic ligands containing pyrimidine unit has high electron affinities and may possibly afford iridium(III) complexes with high quantum efficiency.⁷ These pyrimidine-based iridium(III) complexes have better properties than pyridine-based iridium(III) complexes, so iridium(III) pyrimidine complexes have attracted much attention for their high device performances in the past decade.^{5,8-11} Some new iridium(III) complexes using 2-substituted pyrimidine derivatives as the cyclometalated ligands were synthesized.^{5,8,9} Chang *et al.* designed 5-substituted pyrimidine chelates and the corresponding iridium complexes. With this new phosphor design, the best phosphorescent OLED exhibited a peak external quantum efficiency of 17.9%, a luminance efficiency (LE) of 38.0 cd A⁻¹.¹⁰ Jiang *et al.* used 4,6-disubstituted pyrimidine derivatives as the cyclometalated ligands and synthesized pyrimidine-based iridium(III) complexes with high quantum efficiency.¹¹ Among these pyrimidine-based iridium(III) complexes, ancillary ligands (L^X) are usually containing C, N, O atoms and the most common

^aKey Laboratory for Organic Electronics and Information Displays & Institute of Advanced Materials(IAM), Jiangsu National Synergetic Innovation Center for Advanced Materials (SICAM), Nanjing University of Posts & Telecommunications, 9 Wenyuan Road, Nanjing 210023, China. E-mail: iamqbmei@njupt.edu.cn; iamshye@njupt.edu.cn

^bCollege of Metallurgy and Resources, Anhui University of Technology, Ma'anshan, Anhui 243002, P. R. China

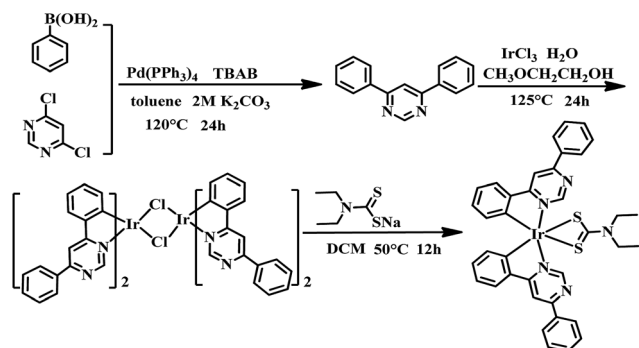
[†] Electronic supplementary information (ESI) available: Experimental details, structure characterization data of the ligands and iridium complexes synthesized in this work, cyclic voltammogram and computational details. CCDC 1402238. For ESI and crystallographic data in CIF or other electronic format see DOI: 10.1039/c6ra12529h

auxiliary ligands are acetylacetonate (acac, $L^X=O^{\wedge}O$), 2-pyridinecarboxylic acid (pic, $L^X=N^{\wedge}O$) and 2,2'-bipyridine (bipy, $L^X=N^{\wedge}N$). Sulfur atoms are rarely introduced into the auxiliary ligands for the iridium complexes used in OLEDs. In recently, the selection of ancillary chelates has been extended to the less accessible, tailor-made heterocycles such as dithiocarbamate, dithiophosphate, and benzamidine. Dithiolate compounds are very stable that can reduce the work function of the emitter and reduce the threshold electric field, therefore reducing the turn on voltage.¹² Iridium(III) complexes (TPQ)₂-Ir(Et₂dtc) and (TPQ)₂-Ir(Et₂dtp) used dithiolate ($S^{\wedge}S$) as the ancillary ligand were synthesized, but two complexes showed low photoluminescence quantum efficiencies of only 8.4% and 3.2%, respectively.^{12,13} In this paper, a highly efficient phosphorescent iridium(III) complex Ir(dpp)₂(dta) with diethyldithiocarbamate ($S^{\wedge}S$) as the ancillary ligand was successfully designed and synthesized with emission ranged at 575 nm and high photoluminescence quantum yield of 86%. We used Ir(dpp)₂(dta) as a triplet emitter doped in a polymeric host (70% PVK: 30% OXD-7) in solution-processed method and prepared yellow-orange OLED. When the doping density was 3%, the device achieved the maximum luminance of 81 918 cd m⁻², the highest EL efficiency of 30.12 cd A⁻¹ and the external quantum efficiency of 9.28%.

Results and discussion

Synthesis and characterization

As shown in Scheme 1, the cyclometalated ligand 4,6-diphenyl pyrimidine was conveniently prepared by 4,6-dichloropyrimidine and phenyl-boronic acid in the toluene solvent according to the Suzuki procedures. The reaction was at 120 °C for 24 h and the yield of products was satisfactory. The synthesis of the iridium(III) complex Ir(dpp)₂(dta) included two steps. First, the cyclometalated Ir(III) μ -chloride bridged dimer was synthesized by reacting IrCl₃·3H₂O with the cyclometalated ligand at 125 °C for 24 h under nitrogen. Then, the chloride-bridged dimer was reacted with sodium diethyldithiocarbamate in dichloromethane (CH₂Cl₂) solution to afford the target products in 60% yields. The structures of these products were confirmed by NMR and mass.



Scheme 1 Synthesis of Ir(dpp)₂(dta).

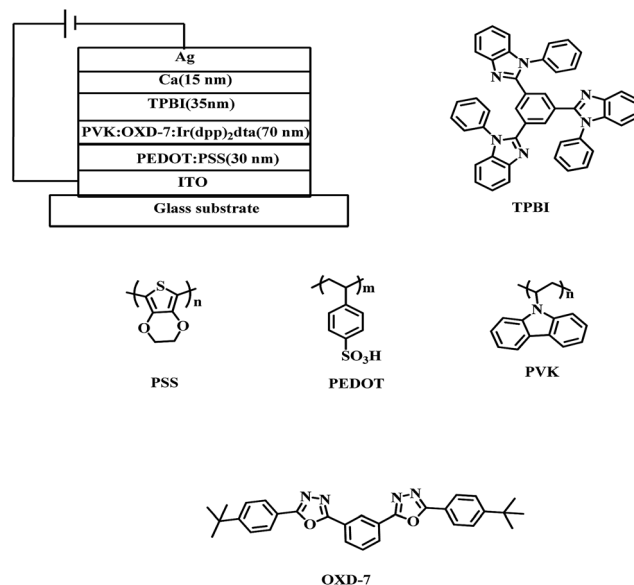


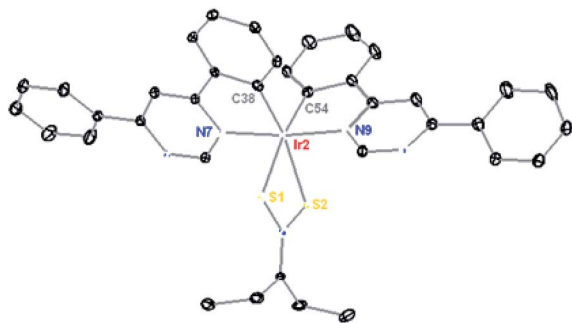
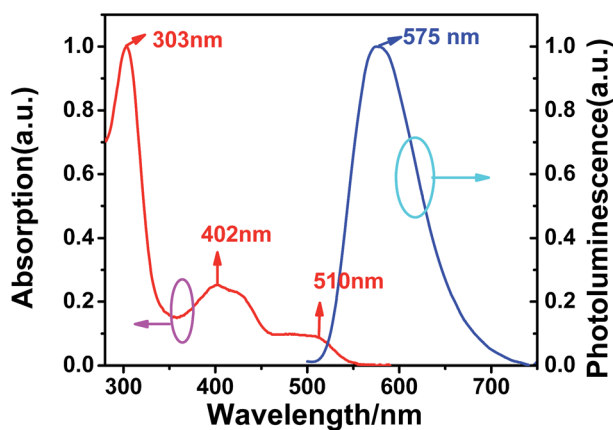
Fig. 1 General structure for the OLED devices and molecular structures of the relevant compounds.

The X-ray crystallography of Ir(dpp)₂(dta)

Single crystal of Ir(dpp)₂(dta) suitable for X-ray diffraction analysis has been grown by slow diffusion of hexane into a dichloromethane solution of the complex. ORTEP drawing of the structure is shown in Fig. 2, and selected crystallographic data are provided in Table S1[†] and the bond lengths [Å] and angles [deg] for Ir(dpp)₂(dta) are listed in Table S2.[†] The complex has the expected octahedral coordination geometry around the iridium center by two cyclometalated ligands 4,6-diphenyl pyrimidine and one ancillary ligand diethyl dithiocarbamic acid sodium salt (dta) with the *cis*-C,C and *trans*-N,N chelating disposition of the original chloro-bridged dimer as reported in related examples.¹⁴ The Ir–C bond lengths are shorter than the Ir–N bond distances as shown in Table S2.[†] This result implies that there is a stronger *trans* influence of the phenyl group over that of the 4,6-diphenyl pyrimidine. The two coordinated S atoms of ancillary ligand reside in the equatorial plane *trans* to the metalated C (dpp) atoms.

UV-vis absorption and photoluminescence properties

The absorption and the photoluminescence spectra of the complex Ir(dpp)₂(dta) in CH₂Cl₂ solution at room temperature were shown in Fig. 3. The strong absorption bands at 303 nm and 402 nm were assigned to the spin-allowed $^1\pi-\pi^*$ transition. In addition, the weak and broad absorption band at 510 nm can be attributed to the typical spin-allowed and spin-forbidden metal-to-ligand charge transfer bands (MLCT). It can be found that the MLCT absorption bands of Ir(dpp)₂(dta) were mostly covered by the emission band of host material (PVK: OXD-7 blend $\lambda_{\text{max}} = 320$ nm). It indicated that the Förster energy can transfer from the singlet-excited states of the host to the MLCT states of the iridium(III) complex Ir(dpp)₂(dta) effectively. PL spectrum of Ir(dpp)₂(dta) in CH₂Cl₂ solution showed a strong

Fig. 2 Perspective view of Ir(dpp)₂(dta).Fig. 3 UV-vis absorption and photoluminescence spectra of Ir(dpp)₂(dta) at the solution of CH₂Cl₂.

yellow-orange phosphorescent emission at 575 nm. The phosphorescence emission of the Ir(dpp)₂(dta) complex was found to mainly originate from the ³MLCT (metal-to-ligand charge transfer) excited states and/or the ligand-centered (LC) ³π-π* excited states.¹⁵ Moreover, the absolute quantum efficiencies (Φ) of Ir(dpp)₂(dta) in solid power and doped PMMA were measured. All data of the photophysical properties were listed in Table S3.† The Φ_{power} and Φ_{film} (in 1% PMMA film) were 14% and 86%, respectively. As showed in Fig. S7,† the phosphorescent life time of Ir(dpp)₂(dta) in film was 0.904 μs .

Electrochemical properties

The electrochemical properties of the iridium(III) complex Ir(dpp)₂(dta) was investigated by cyclic voltammetry in CH₂Cl₂ solution at room temperature using ferrocene as the internal standard. The conventional three-electrode cell with a Pt work electrode of 2 mm diameter, a platinum-wire counter electrode, and a Ag/AgCl reference electrode was employed. The scan rate is 0.1 V s⁻¹. At the end of the experiment, the ferrocene/ferricenium (Fc/Fc⁺) couple was used as the internal standard as shown in Fig. S8.† The HOMO energy levels (eV) of the complex is calculated according to the formula: $-[4.8 + (E_{1/2}^{\text{ox}} - E_{1/2}(\text{Fc}/\text{Fc}^+))]$ eV. The half-wave oxidation potential ($E_{1/2}^{\text{ox}}$) is 0.9 V vs. Ag/AgCl as shown in Fig. S9.† The highest occupied molecular orbital (HOMO) energy level was calculated to be -5.28 eV. The energy gap (E_g) derived

Table 1 Energy levels of Ir(dpp)₂(dta)

Molecule	LUMO _{cal}	HOMO _{cal}	$E_g[\text{cal}]$	Transition
Ir(dpp) ₂ (dta)	-1.8776	-5.0886	3.211	LC/MLCT/LLCT

Table 2 Electronic ground states of Ir(dpp)₂(dta)

Molecule	LUMO	HOMO
Ir(dpp) ₂ (dta)		

from the UV-vis absorption band, calculated according to the formula: $1240/\lambda_{\text{abs}}$. Finally, the lowest unoccupied molecular orbital (LUMO) energy level was calculated according to the formula: $\text{HOMO} + E_g$, and to be -3 eV. It is clear that the HOMO and LUMO levels of the complex are exactly between the HOMO and LUMO levels of PVK (HOMO = -5.8 eV and LUMO = -2.2 eV). So the iridium(III) complex Ir(dpp)₂(dta) can trap both electrons and holes, and resulted in high device efficiency.

Theoretical calculations

To compare the experimentally obtained HOMO/LUMO levels with the theoretical calculation, we have used the B3LYP density functional theory (DFT) to calculate HOMO/LUMO energy levels and the electronic ground states for (dfppy)₂Ir(LN[^]O).¹⁶

As shown in Table 1 and 2, it is obvious that the LUMO of Ir(dpp)₂(dta) is located in diphenyl pyrimidine. However the HOMO of Ir(dpp)₂(dta) distributes in Ir and cyclometalated ligand. The energy transfer consists ($d\pi(\text{Ir}) \rightarrow \pi_{\text{S}^*}^*$) MLCT, ($\pi_{\text{C}^*} \rightarrow \pi_{\text{S}^*}^*$) LLCT and ³LC ($\pi_{\text{C}^*} \rightarrow \pi_{\text{C}^*}^*$), especially between their mixed valence.

Thermal properties

The thermal properties of the iridium complex was examined by thermal gravimetric analysis (TGA) under an N₂ atmosphere at

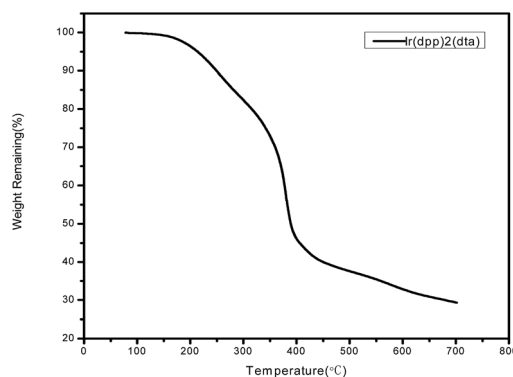


Fig. 4 TG curves of iridium complexes.

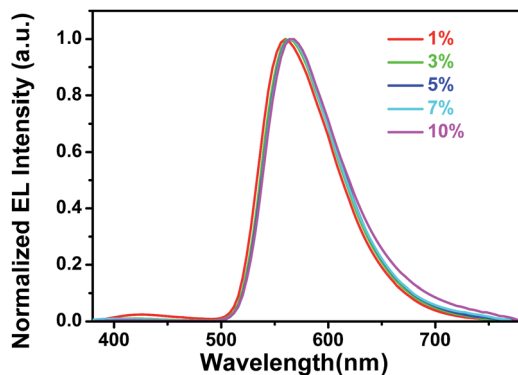


Fig. 5 EL spectra of different devices at 8 V.

a heating rate of $10\text{ }^{\circ}\text{C min}^{-1}$ from room temperature to $700\text{ }^{\circ}\text{C}$. The results in Fig. 4 suggested that $\text{Ir}(\text{dpp})_2(\text{dta})$ exhibited good thermal stability properties with high decomposition temperatures (T_d , corresponding to 5% weight loss) of $215\text{ }^{\circ}\text{C}$, which was beneficial to the long-term stability of the OLED devices fabricated from these materials.

Electrophosphorescent properties

To investigate the EL properties of the iridium(III) complex $\text{Ir}(\text{dpp})_2(\text{dta})$, the PLEDs using $\text{Ir}(\text{dpp})_2(\text{dta})$ as dopant with the device structure of ITO/PEDOT:PSS (40 nm)/(70% PVK + 30% OXD-7): $x\%$ $\text{Ir}(\text{dpp})_2(\text{dta})$ (70 nm)/TPBI (30 nm)/Ca (15 nm)/Ag (100 nm) were fabricated. Fig. 1 shows the general structure and molecular structure of the compounds used in the devices. Indium tin oxide (ITO) on a substrate of electroluminescent device is the anode and Ca/Ag as the cathode. PEDOT:PSS as hole injection layer can smooth the ITO surface, reduce the probability of electrical shorts, decrease the turn-on voltage and prolong the operation lifetime of the device. PVK:OXD-7 blend can be used as host materials, and TPBI as the hole-blocking material can improve electron injection and electron transport. In the emitting layer, the doping concentrations of $\text{Ir}(\text{dpp})_2(\text{dta})$ were 1%, 3%, 5%, 7% and 10%, respectively. The doping concentrations of $\text{Ir}(\text{dpp})_2(\text{dta})$ were according to the

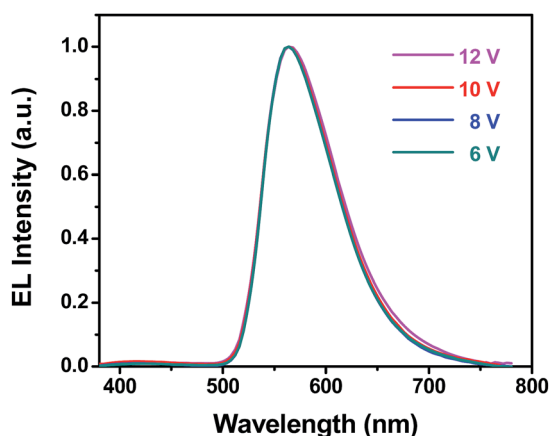


Fig. 6 EL spectra of the device (3%) at different voltage.

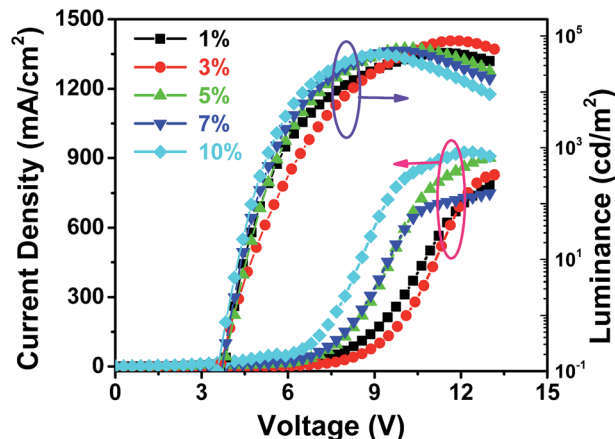


Fig. 7 Current density–voltage–luminance curves of the devices.

host and the mass ratio of OXD-7 was 30% in the PVK:OXD-7 blend.

The HOMO/LUMO levels of the materials used in PLEDs were described in Fig. 1. The PVK:OXD-7 blend material with high HOMO levels as electron-donating and hole-transport media, while TPBI with low LUMO levels as electron-accepting and electron-transport media. Hole was injected from the anode to HOMO levels of host material and electron was injected in LUMO levels. The HOMO and LUMO level of $\text{Ir}(\text{dpp})_2(\text{dta})$ was embedded between the HOMO of PVK (-5.80 eV) and its LUMO (-2.20 eV). Thus, efficient energy transfer to $\text{Ir}(\text{dpp})_2(\text{dta})$ occurred in the emitting layer (EML). The PLED performance in luminance should be determined by the intrinsic quantum efficiency of $\text{Ir}(\text{dpp})_2(\text{dta})$ in radiative decay. Because the HOMO level of $\text{Ir}(\text{dpp})_2(\text{dta})$ was 0.52 eV higher than that of PVK, it behaved as effective trapping sites for holes; meanwhile, the LUMO level of $\text{Ir}(\text{dpp})_2(\text{dta})$ was 0.8 eV lower than that of PVK, electrons injected from the TPBI layer into the emitting layer were mostly transported through the PVK layer and being composited in the iridium phosphor. Thus, varying the concentration of $\text{Ir}(\text{dpp})_2(\text{dta})$ in the EML should significantly alter the degree of charge injection in PVK-based devices.

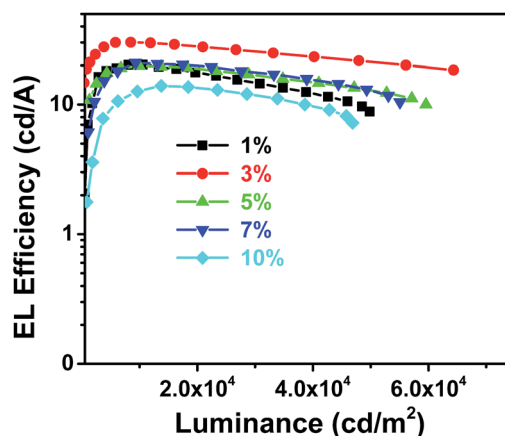


Fig. 8 EL efficiency–luminance of the devices.

Table 3 Performances of the electrophosphorescent devices

Device	Turn-on voltage (V)	L_{\max} (cd m ⁻²)	The maxima of quantum efficiency				Voltage (V)	CD (mA cm ⁻²)	L (cd m ⁻²)	CIE (x, y)
			EQE (%)	LE (cd A ⁻¹)	Roll-off (%) at 20 000 cd m ⁻²					
1(1%)	4	49 804.6	6.16	20.35	13.12	7.68	51.77	10 535.4	(0.4577, 0.5088)	
2(3%)	4.1	81 918.0	9.28	30.12	7.8	8.0	28.18	8488.9	(0.4745, 0.5109)	
3(5%)	4.1	59 649.8	6.02	19.89	4.43	7.09	49.9	9923.4	(0.4792, 0.5074)	
4(7%)	4	55 064.3	6.64	21.01	4.81	6.79	44.34	9318.0	(0.4801, 0.5086)	
5(10%)	3.9	46 857.1	4.61	13.95	6.81	6.8	98.40	13 726.3	(0.4787, 0.5035)	

Therefore, the current density of the PVK-based devices exhibited a strong dependence on the doping concentration.

The normalized electroluminescence (EL) spectra of Ir(dpp)₂(dta) doped PVK:OXD-7 devices in the doping concentrations from 1% to 10% at 8 V are shown in Fig. 5, while others such as 6 V, 10 V and 12 V are in the ESI in Fig. S11.† We noticed that there are weak emission peaks at about 420 nm from the host PVK:OXD-7 in 1% doping concentration. Then the peak decreased with an increase in doping concentration and finally disappeared with increasing doping concentration to 3%. It can be speculated that the energy is complete transfer from host to Ir(dpp)₂(dta) in higher doping concentration. But for the PL spectra for different doping concentrations (Fig. S10†), even at the doping concentration of 7%, complete quenching of the PVK:OXD-7 emission is not observed. This implies that energy transfer from the PVK:OXD-7 blend to the iridium complex is inefficient under photo-excitation. The phenomenon with complete quenching of the host EL emission in higher doping concentration (5–10%) indicating that excitons in the dopants formed both by direct charge trapping in the dopant molecules and energy transfer from the host to Ir(dpp)₂(dta) is efficient under electrical excitation. So the doping concentrations have significant influence on the mixing single and triplet emission of MLCT. EL spectra with peaks at about 575 nm are observed in all of the devices. Meanwhile, with doping concentration increasing, the EL spectra are steadily and the CIE plot were located in the Fig. S13.† The Commission International de l'Éclairage (CIE) color coordinate is (0.4745, 0.5109) which is almost closed to the standard yellow demanded by the National Television System Committee (NTSC). Fig. 6 present selector luminescence spectra of device (3%) at different voltage, while others such as 1%, 5%, 7%, 10% are in the Fig. S12 in ESI.† With the change of voltage from 6 V to 12 V, the spectrum is almost unchanged and there are no residual emissions from the host even at high voltage. It can be indicated that the device had a good light-stability. Fig. 7 shows current density and luminance vs. voltage curves of Ir(dpp)₂(dta) doped OLEDs from 1% to 10% doping concentrations. The device at 3% doping concentration achieved the maximum luminance, reaching 81 918 cd m⁻².

The maximum external quantum efficiency and the maximum luminous efficiency of the device at 3% doping concentration are 9.28% (Fig. S14†) and 30.12 cd A⁻¹ (Fig. 8), respectively. The EL device with a traditional EL structure shows no obvious efficiency roll-off even at high luminance and the EL

efficiency decrease by 7.8% of its maximum upon 20 000 cd m⁻² (Table 3). The extra-high efficiency is an indication of balanced electron and hole recombination in the host matrix, and complete energy and charge transfer from the host material to iridium(III) complex upon electrical excitation. The devices showed no obvious differences in turn-on voltage with increasing doping concentration from 1% to 10%. In order to investigate the performances of these electrophosphorescent devices with different doping concentrations, the parameters of these devices were summarized in Table 3. The best device performance was obtained in the device 2 at 3% doping concentration.

Conclusions

In summary, we designed and synthesized a new iridium(III) complex by introducing the 4,6-diphenylpyrimidine on the frame of Ir(dpp)₂(dta) to develop highly efficient yellow phosphors. In addition, the Ir(dpp)₂(dta)-based device 2 still possessed high EL efficiency of 30.12 cd A⁻¹, maximum luminance of 81 918.0 cd m⁻² and EQE of 9.28% at extremely high luminance of 8488.9 cd m⁻². To the best of our knowledge, this efficiency was a higher ever reported for vacuum-deposited yellow PhOLEDs.

Experimental

The synthesis of Ir(dpp)₂(dta)¹⁷

A mixture of 4,6-dichloro-pyrimidine (0.3 g, 2 mmol), phenylboronic acid (1.08 g, 4 mmol), Pd(pph₃)₄, TBAB, toluene (10 mL) and 2 M K₂CO₃ (10 mL) were stirred at 120 °C for 24 h under nitrogen. Then the reaction mixture was cooled to room temperature, and followed poured into 200 mL water extracted by ethyl acetate. The organic layer was washed with water and dried over anhydrous Mg₂SO₄. After filtration, the solvent was removed under reduced pressure. The residue was purified by column chromatography (petroleum ether/ethyl acetate (6 : 1) as eluent) to afford 4,6-diphenyl pyrimidine, yield = 80%, mp = 80 °C. ¹H NMR (400 MHz, CDCl₃) δ 9.33 (s, 1H), 8.14 (dd, *J* = 13.2, 9.4 Hz, 5H), 7.59–7.50 (m, 6H). ¹³C NMR (CDCl₃, 100 MHz) δ: 164.73, 159.23, 137.05, 130.97, 129.06, 127.22, 112.86. GC-MS (*m/z*): 232.

A mixture of IrCl₃·3H₂O (0.70 g, 2 mmol) and 4,6-diphenylpyrimidine (1.16 g, 5 mmol) were added in a mixture of 2-methoxyethanol 12 mL and distilled water 4 mL. The mixture

was stirred at 125 °C for 24 h under nitrogen. After cooled to room temperature, the precipitate was collected by filtration and washed with water and ethanol, gave to the dimeric iridium(III) complex [(dpp)₂IrCl]₂. After drying, the crude product was directly used for next step without further purification. Cyclometalated [(dpp)₂IrCl]₂ (1.38 g, 1 mmol), K₂CO₃ (1.38 g, 10 mmol) and 5 equivalents of diethyl dithiocarbamic acid sodium salt in dichloromethane (10 mL) was stirred at room temperature under a nitrogen atmosphere for 3 h. After reaction, the mixture solution was distilled under vacuum. The crude product was purified by column chromatography over aluminum oxide using dichloromethane/petroleum ether as the eluent to afford the desired iridium(III) complex Ir(dpp)₂(dta) (4.8 mmol, 2.8 g). Yield: 60%. ¹H NMR (400 MHz, CDCl₃) δ: 10.24 (d, *J* = 0.9 Hz, 2H), 8.27 (dd, *J* = 8.0, 1.3 Hz, 4H), 8.19 (d, *J* = 0.8 Hz, 2H), 7.81 (dd, *J* = 7.8, 0.9 Hz, 2H), 7.64–7.53 (m, 6H), 6.88 (dd, *J* = 7.6, 1.0 Hz, 2H), 6.82 (dd, *J* = 7.5, 1.2 Hz, 2H), 6.62–6.54 (m, 2H), 3.76–3.70 (m, 2H), 3.62–3.46 (m, 2H), 1.25 (d, *J* = 4.8 Hz, 6H). ¹³C NMR (CDCl₃, 100 MHz) δ: 175.17, 162.75, 160.44, 159.96, 144.73, 136.23, 132.42, 131.37, 130.92, 129.05, 127.51, 125.62, 121.19, 109.03, 43.78, 12.40. HRMS (+TOF): *m/z* = 804.1818 (calcd 804 for [C₃₇H₃₂N₃S₂Ir], [M]⁺).

Acknowledgements

The authors acknowledge financial support from the National Basic Research Program of China (973 Program, 2012CB933301, 2012CB723402), the Ministry of Education of China (IRT1148), the National Natural Science Foundation of China (BZ2010043, 20974046, 20774043, 51173081, 50428303, 61106017, 61136003), the Priority Academic Program Development of Jiangsu Higher Education Institutions (PAPD, YX03001), Jiangsu National Synergistic Innovation Center for Advanced Materials (SICAM), the Nature Science Foundation of Jiangsu Province (BK20131375) and the Research Fund for Nanjing University of Posts and Telecommunications (NY215153).

Notes and references

- 1 C. W. Tang and S. A. VanSlyke, *Appl. Phys. Lett.*, 1987, **51**, 913; M. A. Baldo, M. E. Thompson and S. R. Forrest, *Nature*, 1998, **395**, 151.
- 2 M. A. Baldo, S. Lamansky, P. E. Burrows, M. E. Thompson and S. R. Forrest, *Appl. Phys. Lett.*, 1999, **75**, 4.
- 3 B. W. D'Andrade and S. R. Forrest, *Adv. Mater.*, 2004, **16**, 1585.
- 4 C. Fan and C. Yang, *Chem. Soc. Rev.*, 2014, **43**, 6439.
- 5 C. F. Lin, W. S. Huang, H. H. Chou and J. T. Lin, *J. Org. Chem.*, 2009, **694**, 2757.
- 6 A. Tsuboyama, H. Iwawaki, M. Furugori, T. Mukaide, J. Kamatani, S. Igawa, T. Moriyama, S. Miura, T. Takiguchi,

- S. Okada, M. Hoshino and K. Ueno, *J. Am. Chem. Soc.*, 2003, **125**, 12971.
- 7 C. L. Ho, W. Y. Wong, G. J. Zhou, B. Yao, Z. Y. Xie and L. X. Wang, *Adv. Funct. Mater.*, 2007, **17**, 2925.
- 8 G. P. Ge, J. He, H. Q. Guo, F. Z. Wang and D. C. Zou, *J. Org. Chem.*, 2009, **694**, 3050.
- 9 Z. Q. Wang, C. Xu, X. M. Dong, Y. P. Zhang, X. Q. Hao, J. F. Gong, M. P. Song and B. M. Ji, *Inorg. Chem. Commun.*, 2011, **14**, 316.
- 10 C. H. Chang, Z. J. Wu, C. H. Chiu, Y. H. Liang, Y. S. Tsai, J. L. Liao, Y. Chi, H. Y. Hsieh, T. Y. Kuo, G. H. Lee, H. A. Pan, P. T. Chou, J. S. Lin and M. R. Tseng, *ACS Appl. Mater. Interfaces*, 2013, **5**, 7341; J. S. Park, Y. G. Park, J. Y. Lee, J. W. Kang, J. Liu and S. H. Jin, *Org. Electron.*, 2013, **14**, 2114; F. L. Zhang, W. L. Li, Y. M. Jing, D. X. Ma, F. Q. Zhang, S. Z. Li, G. G. Cao, G. Guo, B. Wei, D. P. Zhang, L. Duan, C. Y. Li, Y. F. Feng and B. Zhai, *J. Mater. Chem.*, 2016, DOI: 10.1039/c6tc01041e.
- 11 L. S. Cui, Y. Liu, X. Y. Liu, Z. Q. Jiang and L. S. Liao, *ACS Appl. Mater. Interfaces*, 2015, **7**, 11007.
- 12 D. Q. Gao, F. Scholz, H. G. Nothofer, W. E. Ford, U. Scherf, J. M. Wessels, A. Yasuda and F. V. Wrochem, *J. Am. Chem. Soc.*, 2011, **133**, 5921–5930; Y. Liu, K. Ye, Y. Fan, W. Song, Y. Wang and Z. Hou, *Chem. Commun.*, 2009, **25**, 3699; T. Peng, H. Bi, Y. Liu, Y. Fan, H. Gao, Y. Wang and Z. Hou, *J. Mater. Chem.*, 2009, **19**, 8072.
- 13 L. Q. Chen, H. You, C. L. Yang, X. W. Zhang, J. G. Qin and D. G. Ma, *J. Mater. Chem.*, 2006, **16**, 3332; L. Q. Chen, C. L. Yang, J. G. Qin, J. Gao, H. You and D. G. Ma, *J. Organomet. Chem.*, 2006, **691**, 3519; L. Q. Chen, C. L. Yang, J. G. Qin, J. Gao and D. G. Ma, *Synth. Met.*, 2005, **152**, 225.
- 14 S. Lamansky, P. Djurovich, D. Murphy, F. Abdel-Razzaq, R. Kwong, I. Tsyba, M. Bortz, B. Mui, R. Bau and M. E. Thompson, *Inorg. Chem.*, 2001, **40**, 1704; A. J. Hallett, B. D. Ward, B. M. Kariuki and S. J. A. Pope, *J. Organomet. Chem.*, 2010, **695**, 2401.
- 15 I. M. Dixon, J. P. Collin, J. P. Sauvage, L. Flamigni, S. Encinas and F. Barigelletti, *Chem. Soc. Rev.*, 2000, **29**, 385.
- 16 D. R. Whang, Y. You, S. H. Kim, W. L. Jeong, Y. S. Park, J. J. Kim and S. Y. Park, *Appl. Phys. Lett.*, 2007, **91**, 233501; L. L. Shi, J. J. Su and Z. J. Wu, *Inorg. Chem.*, 2011, **50**, 5477; L. L. Shi, B. Hong, W. Guan, Z. J. Wu and Z. M. Su, *J. Phys. Chem. A*, 2010, **114**, 6559; X. N. Li, Z. J. Wu, Z. J. Si, H. J. Zhang, L. Zhou and X. J. Liu, *Inorg. Chem.*, 2009, **48**, 7740; J. H. Jou, Y. X. Lin, S. H. Peng, C. J. Li, Y. M. Yang, C. L. Chin, J. J. Shyue, S. S. Sun, M. Lee, C. T. Chen, M. C. Liu, C. C. Chen, G. Y. Chen, J. H. Wu, C. H. Li, C. F. Sung, M. J. Lee and J. P. Hu, *Adv. Funct. Mater.*, 2014, **24**, 555.
- 17 Q. B. Mei, Y. H. Guo, B. H. Tong, J. N. Weng, B. Zhang and W. Huang, *Analyst*, 2012, **137**, 5398.